# Low-Temperature Photothermal $CO_2$-to-CO Conversion from Flue Gas Using a g-$C_3N_4$/$TiO_2$/MXene Heterojunction with 100% Selectivity

Yang Meng [a,b], Wen Li [a], Silvia Zamponi [b], Yongpeng Ma [a], Weifeng Zhou [c], Hongxia Chao [c], Shi Tang [c], Mario Berrettoni [b,*], Hongzhong Zhang [a,*]

[a] Henan Collaborative Innovation Center of Environmental Pollution Control and Ecological Restoration, Zhengzhou University of Light Industry, Zhengzhou 450001, China

[b] Department of Chemistry, University of Camerino, 62032 Camerino, Macerata, Italy

[c] Zhengzhou Ecological Environment Monitoring Center of Henan Province, China

[*] Correspondence: zhz@zzuli.edu.cn (H.Z.); mario.berrettoni@unicam.it (M.B.)

## 2. Experimental

## 2.1 Reagents

Titanium isopropoxide ($C_{12}H_{28}O_4Ti$, AR, 99%), isopropanol ($C_3H_8O$, AR, 99.7%), titanium aluminum carbide ($Ti_3AlC_2$, AR, 98%), and urea ($H_2NCONH_2$, AR, 99%) were purchased from Aladdin Chemical Reagent Co., Ltd. Acetic acid ($CH_3COOH$, AR, 99.5%) and hydrofluoric acid (HF, AR, 40%) were purchased from Tianjin Fengchuang Chemical Reagent Co., Ltd., and all reagents were used as received without further purification.

## 2.2 Synthesis and characterization

### 2.2.1 Preparation of MXene

MXene was prepared via selective etching of $Ti_3AlC_2$.[1] Typically, 5 g of $Ti_3AlC_2$ powder was slowly added to 80 mL of HF in a plastic beaker under rapid stirring and then maintained at 60 °C in an oil bath for 72 h. After natural cooling to room temperature, the suspension was repeatedly washed with deionized water until the supernatant reached neutral pH, followed by several washes with anhydrous ethanol. The obtained product was vacuum-dried at 60 °C overnight to yield MXene.

### 2.2.2 Synthesis of g-$C_3N_4$

g-$C_3N_4$ was synthesized via a thermal polymerization method.[2] In a typical procedure, 10 g of urea was placed in an alumina crucible sealed with aluminum foil and heated to 550 °C in a muffle furnace under static air for 3 h. After natural cooling, the product was washed with deionized water and ethanol, dried at 60 °C overnight, and collected as g-$C_3N_4$.

### 2.2.3 Synthesis of $TiO_2$/MXene

First, 5 mL of titanium isopropoxide was added to 20 mL of isopropanol and ultrasonicated for 30 min to obtain solution A. Separately, 4 mL of acetic acid was added to 8 mL of isopropanol and ultrasonicated for 30 min to obtain solution B. Under vigorous stirring, solution B was slowly dropped into solution A and stirred at room temperature for 24 h to form a Ti sol. Subsequently, a methanolic dispersion of MXene was introduced into the Ti sol and stirred at room temperature for another 24 h. The mixture was vacuum-dried overnight at 100 °C and then annealed in a muffle furnace at 500 °C for 2 h under an argon atmosphere to obtain $TiO_2$/MXene (TM).

### 2.2.4 Synthesis of g-$C_3N_4$/$TiO_2$/MXene

Following the procedure described above for Ti sol preparation, 0.2 g of g-$C_3N_4$ and varying amounts of MXene (0.19 g, 0.285 g, 0.38 g, and 0.475 g) were co-dispersed in methanol and stirred at room temperature for 24 h. The suspension was then added dropwise into the pre-formed Ti sol and further stirred at room temperature for another 24 h. After vacuum drying at 100 °C overnight, the precursor was annealed at 500 °C for 2 h under an argon atmosphere to yield g-$C_3N_4$/$TiO_2$/MXene (GTM) composites, denoted as GTM-1, GTM-2, GTM-3, and GTM-4.

### 2.2.5 Characterization

The crystal structure and functional groups of the catalysts were characterized by X-ray diffraction (XRD; Bruker D8 ADVANCE) and Fourier transform infrared spectroscopy (FTIR; Thermo Fisher Nicolet iS10). The microstructure and elemental distribution were analyzed using scanning electron microscopy (SEM; JSM-7001F), energy-dispersive X-ray spectroscopy (EDS), and high-resolution transmission electron microscopy (HRTEM; FEI TF20). The specific surface area, pore size distribution, and $CO_2$ adsorption-desorption properties were measured by Brunauer-Emmett-Teller (BET) analysis (Maxwell 2640). UV-vis diffuse reflectance

spectroscopy (UV-vis DRS; UH-4150) was employed to investigate the optical absorption properties and estimate the band structures of the samples. Raman spectroscopy was used to analyze the chemical structure of the materials. Surface chemical composition and valence states were examined by X-ray photoelectron spectroscopy (XPS; ESCALAB 250Xi). The charge carrier dynamics were probed using steady-state and time-resolved photoluminescence spectroscopy (PL; Edinburgh FLS1000). Thermogravimetric infrared spectroscopy (TG-IR; METTLER TGA2 coupled with SEMERFIELD iS50) and in situ FTIR were performed to evaluate the thermal stability of the catalysts and to identify the intermediate species and products formed during $CO_2$ reduction. Electrochemical impedance spectroscopy (EIS) and photocurrent response measurements were carried out using an electrochemical workstation (CHI660E, Chenhua, Shanghai). The composition, content, and isotopic distribution of the gaseous products were analyzed by gas chromatography (GC; Techcomp GC-7980, Shanghai) and gas chromatography-mass spectrometry (GC-MS; Agilent 7980A-5975C).

### 2.3 Theoretical calculations

We have employed the Vienna Ab initio Simulation Package (VASP) [3, 4] to perform all density functional theory (DFT) calculations within the generalized gradient approximation (GGA) using the Perdew-Burke-Ernzerhof (PBE) [5] functional. We have chosen the projected augmented wave (PAW) potentials [6, 7] to describe the ionic cores and take valence electrons into account using a plane wave basis set with a kinetic energy cutoff of 450 eV. The DFT-D3 empirical correction method was employed to describe van der Waals interactions. Geometry optimizations were performed with the force convergency smaller than 0.05 eV/Å and the energy convergence of $1 \times 10^{-5}$ eV. Besides, (2×2×1), (10×10×1), (2×2×1) and (2×2×1) k-point sampling with the Monkhorst-Pack mesh was used for the Brillouin zone integration for g-$C_3N_4$, $Ti_3C_2O_2$, $TiO_2$ cluster and g-$C_3N_4$/$Ti_3C_2O_2$/$TiO_2$, respectively. After geometry optimization, the work function, bader charge and Charge-Density Difference were calculated with the

Monkhorst-Pack mesh of (4×4×1), (19×19×1), (4×4×1) and (4×4×1) for g-$C_3N_4$, $Ti_3C_2O_2$, $TiO_2$ cluster and g-$C_3N_4$/$Ti_3C_2O_2$/$TiO_2$, respectively.

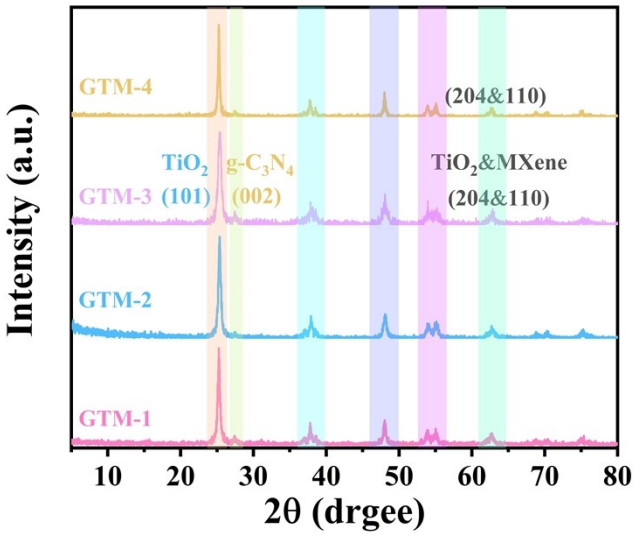


Fig. S1. XRD patterns of GTM.

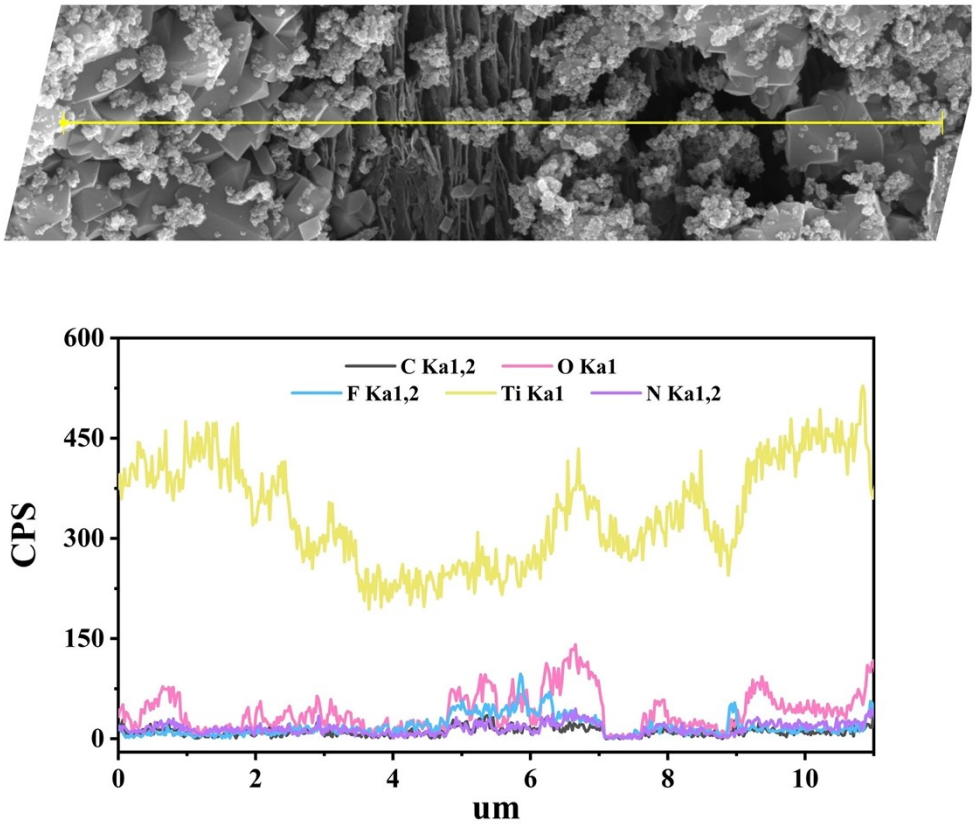


Fig. S2. SEM and EDS images of GTM.

Table S1.

Photothermal conversion performance of different catalysts.

| Time / Samples | 0s | 30s | 60s | 90s | 150s |
|---|---|---|---|---|---|
| g-$C_3N_4$ | 28.3 °C | 30.1 °C | 31.1 °C | 31.3 °C | 31.4 °C |
| $TiO_2$ | 28.5 °C | 32.1 °C | 32.7 °C | 32.9 °C | 33.2 °C |
| MXene | 28.3 °C | 37.7 °C | 39.1 °C | 39.9 °C | 40.7 °C |
| TM | 28.4 °C | 32.9 °C | 33.7 °C | 34.1 °C | 34.8 °C |
| GTM | 28.4 °C | 33.4 °C | 34.3 °C | 34.7 °C | 35.5 °C |

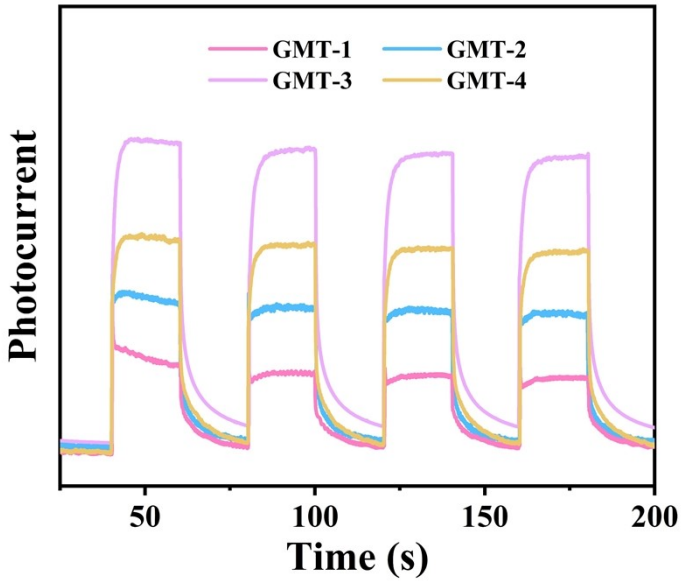


Fig. S3. Photocurrent response spectra of GTM.

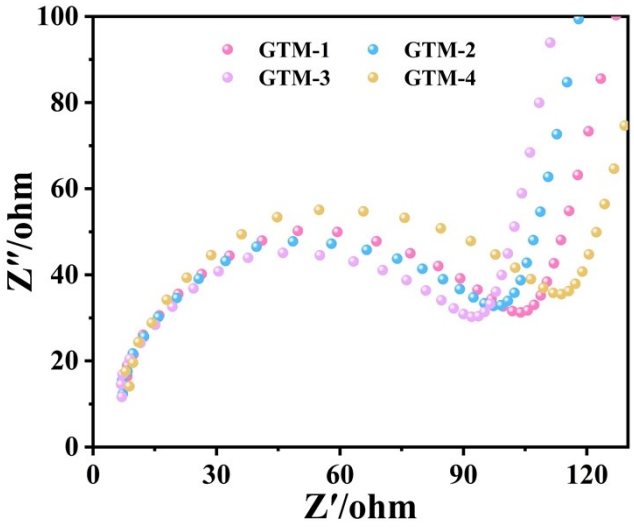


Fig. S4. EIS diagram of GTM.

Table S2.

Comparison with recently reported MXene-based low-temperature photothermal systems and flue-gas-compatible catalysts.

| Catalysts | Gas source | Reaction condition | Yield and Selectivity | Ref |
|---|---|---|---|---|

| | | | ($\mu mol \cdot g^{-1} \cdot h^{-1}$) | |
|---|---|---|---|---|
| BT@Ag | $CO_2$+$H_2O$ | 300W Xe~101 °C | CO: 2.3 ~ 50.0%<br>$CH_4$: 2.3 ~ 50.0% | [8] |
| dTOCN | $CO_2$+$H_2O$ | 300W Xe+30 °C | CO: 11.4 ~ 100.0% | [9] |
| MXene/$SiO_2$-$CeO_2$ | $CO_2$+$H_2O$ | 300W Xe+100 °C | CO: 4.8 ~ 73.8%<br>$CH_4$: 1.7 ~ 26.2% | [10] |
| BiOI/$Ti_3C_2$ | $CO_2$+$H_2O$ | 300W Xe+55 °C | CO: 89.3 ~ 100.0% | [11] |
| Co-MOF MNSs | Industrial flue gas (14.7% $CO_2$) | 300W Xe+TEOA | HCOOH: 850.0 ~ / | [12] |
| g-anatase | Industrial flue gas (10.0% $CO_2$) | 300W Xe+80 °C | CO: 0.8 ~ / | [13] |
| Ti-EBCD | Industrial flue gas (15.0% $CO_2$) | 300W Xe | CO: 18.8 ~ 97.8% | [14] |
| COF1-g-$C_3N_4$ | Industrial flue gas (20.0% $CO_2$) | 300W Xe+TEOA | CO: 166.0 ~ 65.0% | [15] |
| GTM | Industrial flue gas (10.0% $CO_2$) | 300W Xe+80 °C | CO: 349.3 ~ 100.0% | This work |

Table S3.

Surface Temperature of Catalysts Under Different Conditions.

| Catalysts | Initial Temperature (°C) | Reaction Conditions | 1h (°C) | 2h (°C) | 3h (°C) | 6h (°C) |
|---|---|---|---|---|---|---|
| g-$C_3N_4$ | 20.3 | Sunlight | 33.8 | 33.5 | 34.9 | 35.6 |
| $TiO_2$ | 20.1 | Sunlight | 35.6 | 37.8 | 39.1 | 40.9 |
| MXene | 20.3 | Sunlight | 49.2 | 51.2 | 52.8 | 54.3 |
| TM | 20.1 | Sunlight | 43.3 | 43.1 | 46.2 | 48.8 |
| | 20.2 | Sunlight | 43.3 | 45.1 | 46.9 | 49.7 |
| GTM | 20.2 | 80 °C | 69.5 | 71.1 | 70.6 | 71.8 |
| | 20.3 | Sunlight+80 °C | 84.3 | 88.6 | 90.2 | 93.8 |

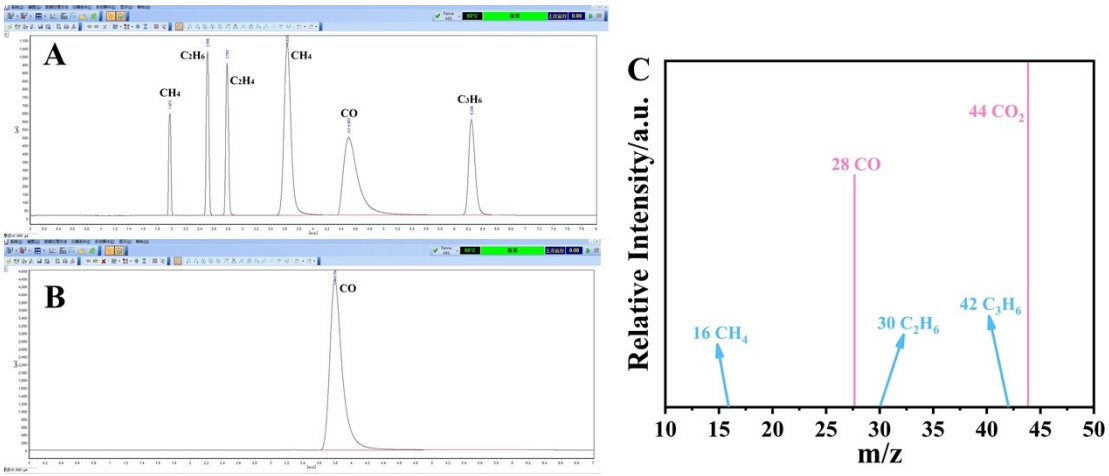


Fig. S5. GC-MS analysis: (A) Standard gas; (B) and (C) Gaseous products collected after 6 h of photothermal $CO_2$ reduction over the GTM catalyst.

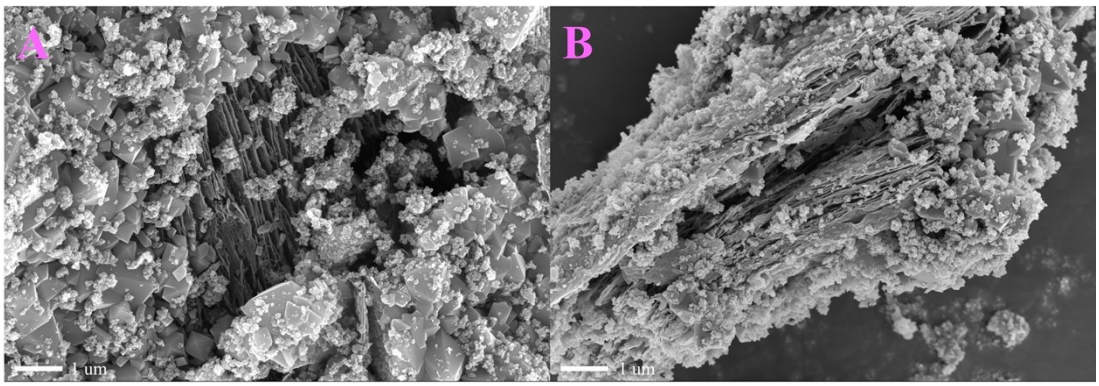


Fig. S6. SEM images of GTM: A. Before reaction; B. After reaction.

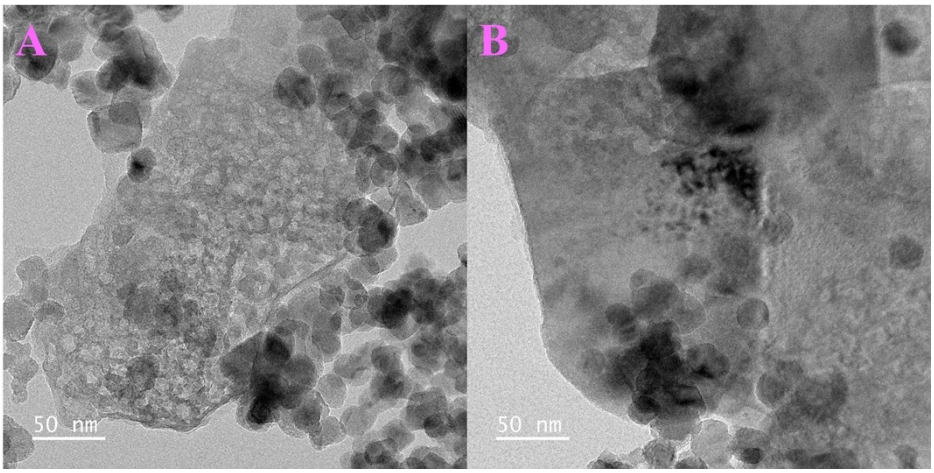


Fig. S7. TEM images of GTM: A. Before reaction; B. After reaction.

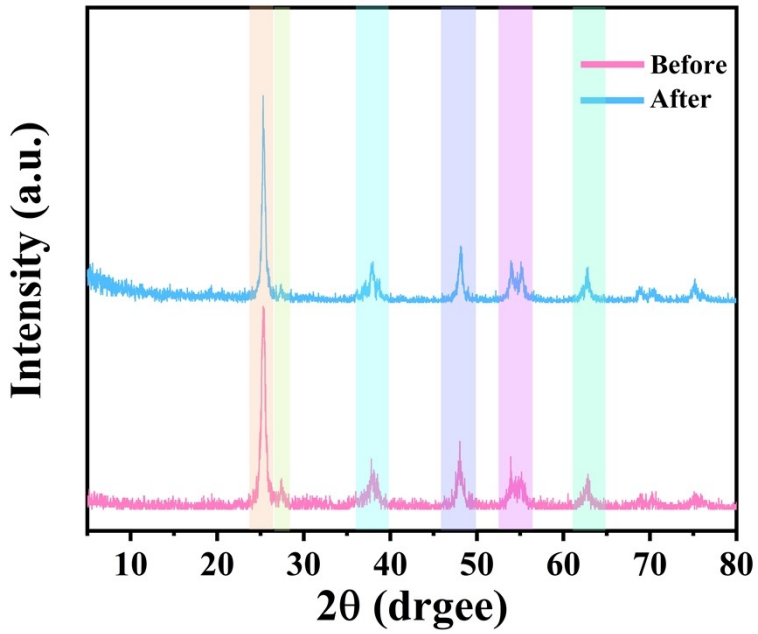


Fig. S8. XRD spectra before and after GTM reaction.

The characteristic peaks of MXene, $TiO_2$, and g-$C_3N_4$ in GTM remain well preserved after the reaction, with no significant changes in intensity and no detectable phase transformation or oxidation of MXene.

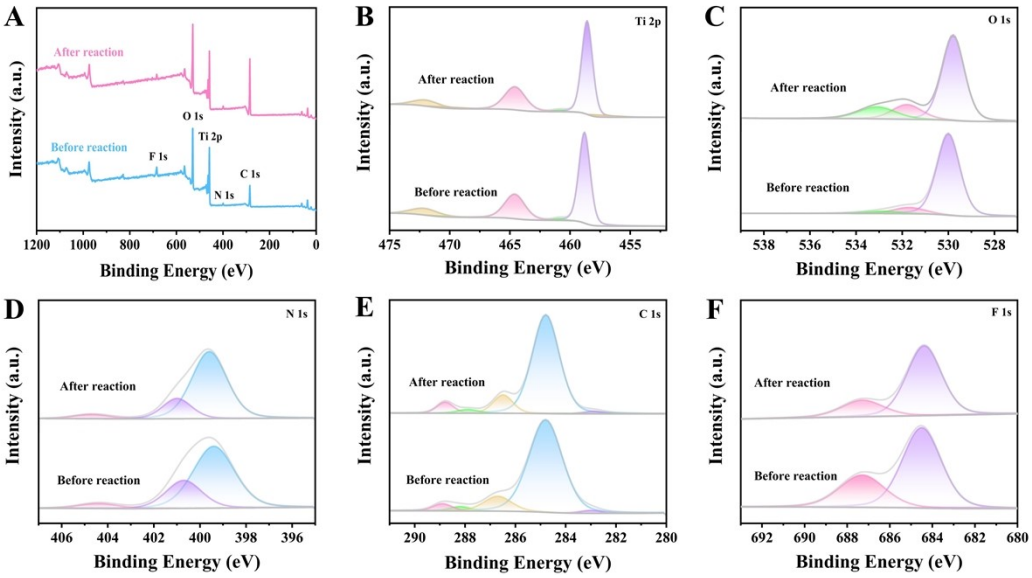


Fig. S9. XPS spectra before and after GTM reaction.

The Ti 2p and C 1s core levels remain unchanged after the reaction, with no significant increase in Ti-O or Ti-OH species—typically indicative of MXene oxidation.

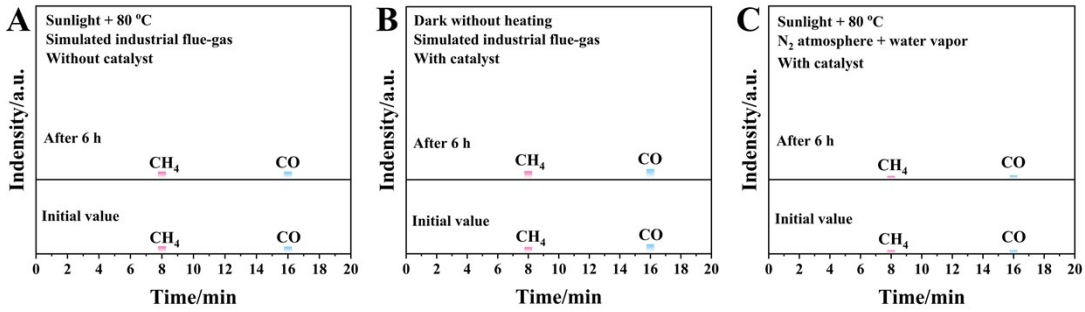


Fig. S10. Control experiments: A. Sunlight + 80 °C, simulated industrial flue-gas and without catalyst; B. Dark without heating, simulated industrial flue-gas and with catalyst; C. Sunlight + 80 °C, $N_2$ atmosphere + water vapor and with catalyst.

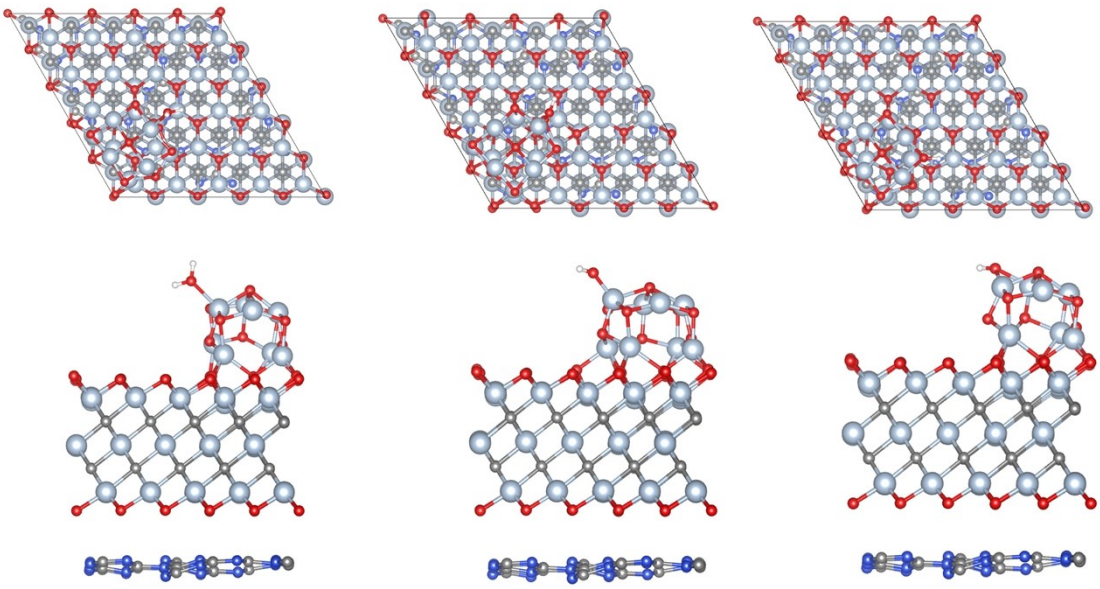

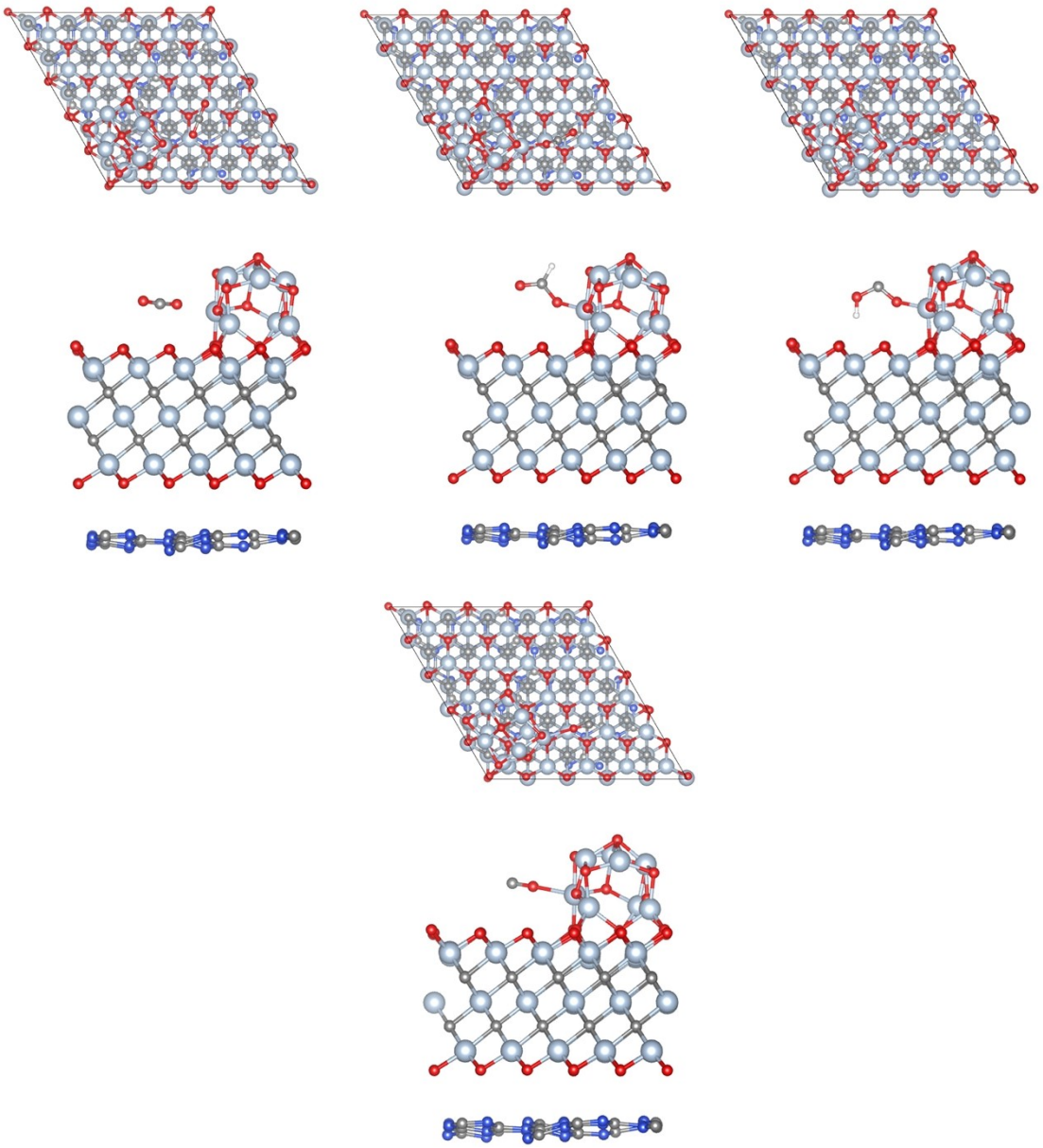

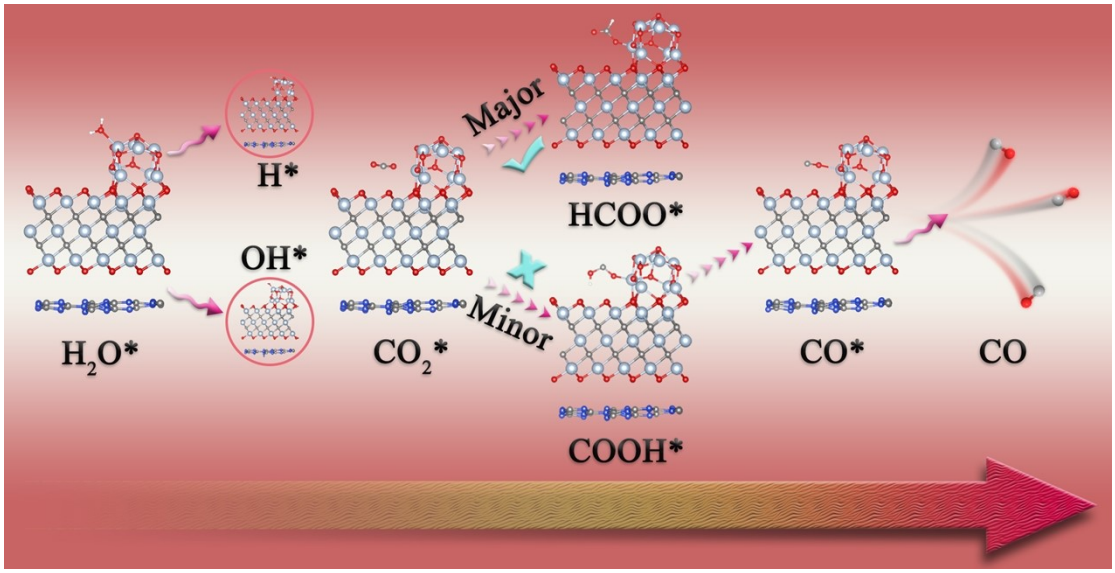


Fig. S11. GTM thermal catalytic $CO_2$ reduction pathway and molecular configuration.

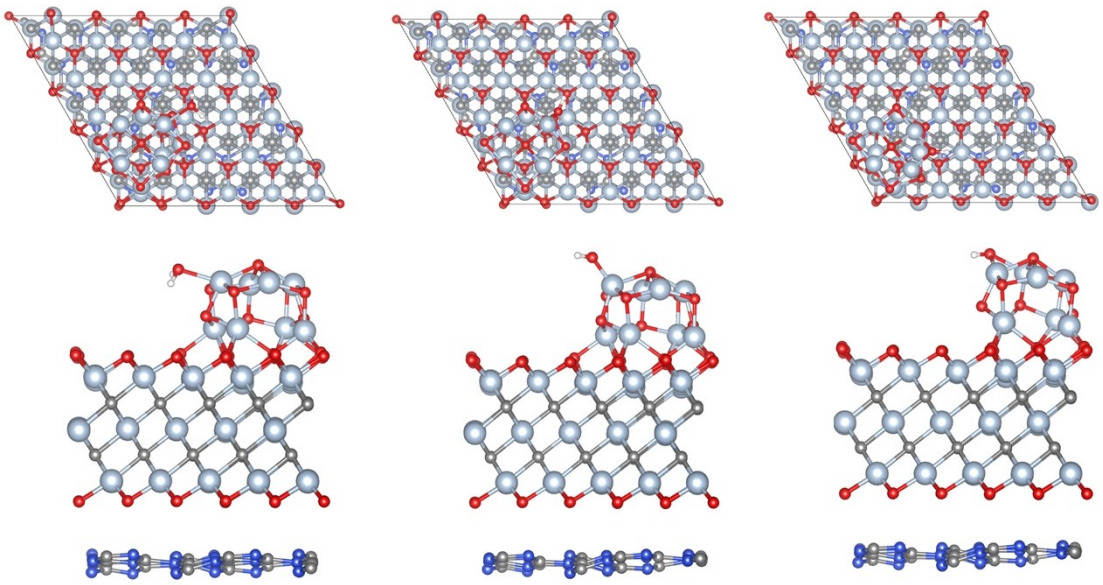

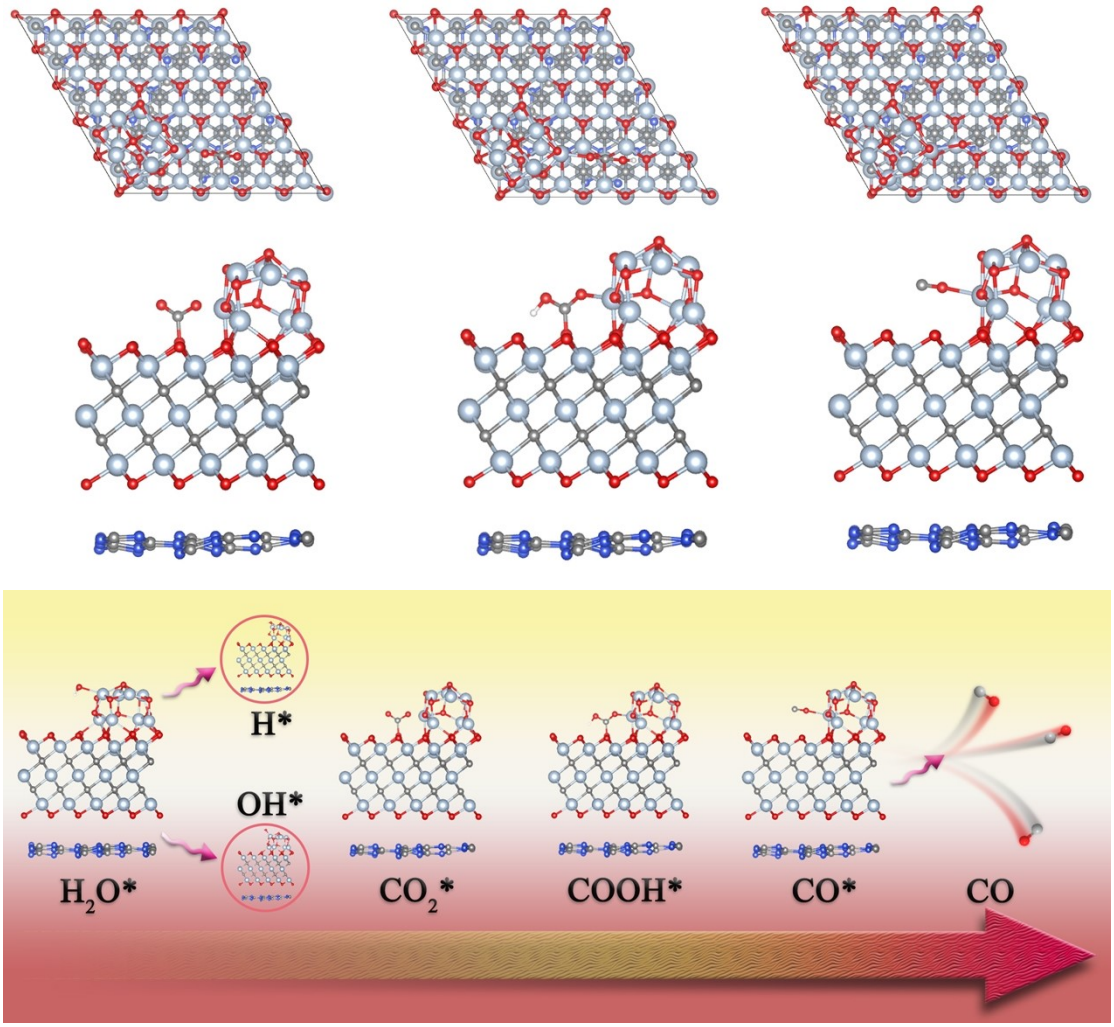


Fig. S12. GTM photocatalysis and photothermal $CO_2$ reduction pathways and molecular configurations.

Table S4.

Gibbs free energy (ΔG) of $CO_2$ catalytic reduction under different conditions of GTM.

| Process | Reaction | ΔG (eV) | | |
|---|---|---|---|---|
| | | Thermal | Sunlight | Photothermal |
| 1 | $CO_2 \rightarrow CO_2^*$ | -0.710 | -1.512 | -1.374 |
| 2 | $H_2O \rightarrow H_2O^*$ | -0.542 | -0.929 | -1.028 |
| 3 | $H_2O^* \rightarrow H^* + OH^*$ | -1.934 | -1.649 | -1.689 |
| 4 | $CO_2^* + H^* \rightarrow HCOO^*$ | -2.110 | / | / |
| 4 | $CO_2^* + H^* \rightarrow COOH^*$ | 1.172 | 0.522 | 0.522 |
| 5 | $COOH^* + H^* \rightarrow CO^* + H_2O^*$ | 0.082 | 0.921 | 0.810 |
| 6 | $CO^* \rightarrow CO$ | 0.906 | 0.526 | 0.349 |

## Reference


1. Y. Meng, W. Li, H. Zhang, J. Yu, Z. Xiao, M. Berrettoni, J. Li, Y. Ma and H. Zhang, J Colloid Interface Sci, 2025, 691, 137405.
2. D. Zhou, J. Zhang, Z. Jin, T. Di and T. Wang, Chemical Engineering Journal, 2022, 450.
3. G. Kresse and J. Furthmüller, Comput. Mater. Sci., 1996, 6, 15-50.
4. G. Kresse and J. Hafner, Phys. Rev. B, 1994, 49, 14251-14269.
5. J. P. Perdew, K. Burke and M. Ernzerhof, Phys. Rev. Lett., 1996, 77, 3865-3868.
6. P. E. Blöchl, O. Jepsen and O. K. Andersen, Phys. Rev. B, 1994, 49, 16223-16233.
7. G. Kresse and D. Joubert, Phys. Rev. B, 1999, 59, 1758-1775.
8. Y. Zhao, Z. Wang, W. Chen, X. Wang, Y. Tang, L. Li and J. Wang, J Colloid Interface Sci, 2025, 683, 934-941.
9. C. Zhu, M. Guo, Z. Wang, J. He, J. Qiu, Y. Guo, Y. Yan, J. Ran and Z. Yang, Catalysts, 2024, 14.
10. G. Dativo, J. Perez-Carvajal, S. Scirè, G. Compagnini, R. Fiorenza and E. Ruiz-Hitzky,

Catalysts, 2026, 16.
11. T. Li, R. Tao, D. Li, D. Liu, S. Zhou, Z. Chu and X. Fan, Applied Surface Science, 2025, 712.
12. D. He, Q. Wang, Y. Rong, Z. Xin, J. J. Liu, Q. Li, K. Shen and Y. Chen, Adv Mater, 2024, 36, e2403920.
13. Y. Guan, M. Xia, A. Marchetti, X. Wang, W. Cao, H. Guan and X. Kong, Catalysts, 2018, 8.
14. G. Zhou, C. Bi, X. Qian, Y. Chen, H. Liu, X. Ning, C. Xue, P. Ding, X. Wang and X. Zhu, ACS Catalysis, 2025, 15, 15972-15981.
15. J. Zhou, M. Dong, Y. Sun, G. G. Shan, C. Y. Sun, S. Q. You, X. L. Wang, Z. H. Kang and Z. M. Su, ACS Appl Mater Interfaces, 2022, 14, 6476-6483.